Hydration Structure of Na^+ and K^+ Ions in Solution Predicted by Data-Driven Many-Body Potentials

Debbie Zhuang,[†,§] Marc Riera,[†,§] Ruihan Zhou,[†] Alexander Deary,[†] and Francesco Paesani[*,†,‡,¶]

†*Department of Chemistry and Biochemistry, University of California San Diego, La Jolla, California 92093, United States*

‡*Materials Science and Engineering, University of California San Diego, La Jolla, California 92093, United States*

¶*San Diego Supercomputer Center, University of California San Diego, La Jolla, California 92093, United States*

§*These authors contributed equally*

E-mail: fpaesani@ucsd.edu

Abstract

The hydration structure of Na^+ and K^+ ions in solution is systematically investigated using a hierarchy of molecular models that progressively include more accurate representations of many-body interactions. We found that a conventional empirical pairwise additive force field that is commonly used in biomolecular simulations is unable to reproduce the extended X-ray absorption fine structure (EXAFS) spectra for both ions. In contrast, progressive inclusion of many-body effects rigorously derived from the many-body expansion of the energy allows the MB-nrg potential energy functions (PEFs) to achieve nearly quantitative agreement with the experimental EXAFS spectra, thus enabling the development of a molecular-level picture of the hydration structure of both Na^+ and K^+ in solution. Since the MB-nrg PEFs have already been shown to accurately describe isomeric equilibria and vibrational spectra of small ion–water clusters in the gas phase, the present study demonstrates that the MB-nrg PEFs effectively represent the long-sought-after models able to correctly predict the properties of ionic aqueous systems from the gas to the liquid phase, which has so far remained elusive.

INTRODUCTION

A microscopic characterization of the hydration properties of alkali-metal ions in solution is key to understanding a wide range of chemical and biochemical processes.[1,2] In this context, aqueous solutions of sodium (Na^+) and potassium (K^+) ions are particularly relevant given the central roles that these two ions play in several physiological functions.[3] For example, Na^+/K^+ pumps serve to maintain the cell membrane potential,[4] provide a gradient to modulate Na^+ transport,[5] regulate the cell volume,[6] function as signal transducers,[7] and control neuron activity states.[8,9] In addition, sodium and potassium ion batteries have recently attracted significant interest as large-scale energy storage systems that are less expensive and more environmentally friendly than current lithium-based technologies.[10,11]

In general terms, the hydration structure of an ion depends on the subtle competition between ion–water and water–water interactions, which is further modulated by entropic effects and possibly nuclear quantum effects. Several molecular models have been developed to describe the interactions of Na^+ and K^+ ions with water, including nonpolarizable and polarizable force fields, *ab initio*-based models, and data-driven many-body potentials, which are then used in molecular dynamics (MD) and Monte Carlo (MC) simulations to investigate structural, thermodynamic, and dynamical properties of various aqueous solutions. In parallel, electronic structure calculations performed at different levels of theory as well as *ab initio* molecular dynamics (AIMD) simulations using various flavors of density functional theory (DFT) have been extensively used to model the hydration structure of Na^+ and K^+ in both aqueous clusters and solutions.

Polarizable and nonpolarizable force fields derived from electronic structure calculations were used to characterize the energetics of small $K^+(H_2O)_n$ clusters as well as the hydration properties of K^+ in solution.[12] Subsequent calculations carried out for $Na^+(H_2O)_n$[13] and $K^+(H_2O)_n$[14] clusters using nonpolarizable force fields identified $n = 20$ as a magic number. Electronic structure calculations performed for $Na^+(H_2O)_n$ and $K^+(H_2O)_n$ clusters with up to 6 water molecules found appreciable differences between sequential binding energies obtained at the DFT (with the B3LYP functional) and MP2 levels of theory.[15] DFT calculations carried out with the B3LYP functional for $K^+(H_2O)_n$ clusters ($n = 1 - 8$) in both gas phase and dielectric media found that the stability and size of the clusters are very sensitive to dielectric effects.[16] Electronic structure calculations carried out for $Na^+(H_2O)_n$ clusters at the MP2 level of theory, which were complemented with analyses performed using the quantum theory of atoms in molecules (QTAIM), found that the average Na^+–O distance decreased as a function of the coordination number from small clusters to bulk solutions.[17]

From clusters to bulk solvation, several theoretical studies have focused on calculating hydration free energies. Pioneering MC simulations carried out with *ab initio*-based force fields derived from configuration interaction and self-consistent field calculations predicted

hydration free energies that differed by 20-30% from the corresponding experimental values, although the general trend was consistent with the measurements.[18] Nonpolarizable force fields were used in MC simulations to determine hydration free energies of various ions, including Na^+ and K^+.[19] It was found that negative ions were solvated more strongly compared to positive ions of equal size due to stronger interactions with the hydrogen atoms of the water molecules. Absolute hydration free energies for Na^+ and K^+ calculated from MD simulations carried out with the AMOEBA polarizable force field were found to be in better agreement with the experimental data than the corresponding values obtained with nonpolarizable force fields.[20] MD simulations with polarizable force fields for Na^+ and K^+ in water, which explicitly included charge transfer, provided hydration free energies and diffusion constants in good agreement with the experimental data.[21] It was also found that, due to charge transfer, water molecules in the first hydration shells of the two ions acquire a partial negative charge.

Different methods were used to study the hydration shell structure around Na^+ and K^+, especially the transition between hydration shells. MC simulations were carried out using a hybrid model where a single Na^+ ion described quantum mechanically was solvated by 89 water molecules represented by a polarizable model, and the entire system was then immersed in a dielectric continuum.[22] These MC simulations found that the coupling between exchange-repulsion and induction energy contributions played a negligible role in determining the hydration structure of Na^+. Quantum mechanics/molecular mechanics (QM/MM) simulations indicated that nonadditive forces significantly affected the properties of the first hydration shell around Na^+ and K^+ in solution, providing evidence for the structure-making and structure-breaking behavior of Na^+ and K^+.[23,24] AIMD simulations within the generalized gradient approximation (GGA) were used to determine the hydration structure and diffusion coefficient of Na^+ in water.[25] Combining quasi-chemical theory (QCT) and AIMD simulations, it was found that $\sim$6 water molecules resided in the first hydration shell of K^+, with the first four molecules forming an inner core and the remaining two molecules

appearing as a shoulder in the calculated K^+-O radial distribution function (RDF).[26] The hydration structure of K^+ was also characterized using MD simulations carried out with both nonpolarizable and polarizable force fields as well as AIMD simulations performed with the BLYP functional.[27] All models were found to predict a similar hydration structure, displaying a first peak in the K^+-O RDF at ∼2.7 Å. Interestingly, both AIMD and MD simulations with the polarizable force field predicted the average induced dipole moment of the water molecules in the first hydration shell to be smaller than the corresponding value calculated for water molecules in the bulk. Subsequent AIMD simulations carried out with the BLYP functional found that the dipole moment of the water molecules residing in the first hydration shell of K^+ decreased with increasing number of molecules, which was explained by considering that the additional water molecules effectively suppress the ion's electric field.[28] Importantly, further addition of water molecules beyond the first hydration shell was found to increase the dipole moment of the molecules in the first hydration shell due to polarization effects associated with the formation of water–water hydrogen bonds.

It is established that the variation of the coordination number as a function of the distance from the ion provides direct insights into the local structure of individual hydration shells. Nonpolarizable force fields were used in MD simulations to characterize the kinetics of water exchange in the first hydration shell of Na^+,[29] as well as in MC simulations to investigate possible relationships between the hydration structure of Na^+ and K^+ in solution and the observed ion specificity of biological channels.[30] MD simulations carried out with polarizable force fields found coordination numbers of 6.39 and 6.89 for Na^+ and K^+ in solution, respectively.[31] AIMD simulations carried out with the BLYP functional for K^+ in solution found that the coordination number increased from 6.24 at 300 K to 6.53 at 450 K.[32] Subsequent DFT-based AIMD simulations carried out with various functionals found that the addition of an empirical dispersion energy term improved the agreement with the measured coordination numbers for both Na^+ and K^+ in solution.[33] The coordination number of K^+ in solution was predicted to be 7.0 and 6.3 from MD simulations carried out with a

conventional QM/MM scheme and the ONIOM-XS method, respectively.[34] QM/MM simulations carried out using the flexible inner region ensemble separator (FIRES) scheme where the QM region was described at the RI-MP2 and DFT (with the PBE functional) levels of theory, and the MM region described by the polarizable SWM4-NDP force field, found that the coordination numbers for Na^+ and K^+ in solution were within the ranges of 5.7-5.8 and 6.9-7.0, respectively.[35] Similar values for the coordination numbers of Na^+ and K^+ in solution were obtained from QM/MM simulations where the ion was described quantum mechanically using the B3LYP functional and the water molecules were represented by the TIP3P model.[36]

More recently, nonpolarizable force fields that effectively account for polarization effects within the electronic continuum correction with rescaling (ECCR) scheme were developed for Na^+[37] and K^+.[38] Building on these studies, a general nonpolarizable force field for ions in water (denoted as Madrid-2019), which adopts scaled charges, was shown to provide a reliable description of several thermodynamic properties of ionic aqueous solutions.[39] A new set of nonpolarizable force fields developed for several ions, including Na^+ and K^+, using a global optimization procedure, were shown to reproduce the concentration-dependent density, ionic conductivity, and dielectric constant of various electrolyte solutions.[40] Polarizable force fields compatible with the BK3 water model were recently shown to reproduce the thermodynamic properties of both salt crystals and ionic aqueous solutions, although they predicted smaller solution enthalpies and self-diffusion constants compared to the experimental values.[41]

Direct information about the hydration structure of ions in solution is obtained from extended X-ray absorption fine structure (EXAFS) spectra. A polarizable force field was used in MD simulations to calculate the EXAFS spectrum of K^+ in water, which was found to be in qualitative agreement with the experimental results.[42,43] Subsequent AIMD simulations carried out with the revPBE and BLYP functionals for Na^+ in solution predicted a Na^+–O distance that was too long with respect to the experimental estimate derived from the EXAFS measurements.[44] Interestingly, in the same study, it was also found that the addition

of an empirical dispersion energy term to the DFT models resulted in a worse agreement with the experimental values, while a nonpolarizable force field predicted the correct Na^+–O distance but overestimated the overall hydration structure. Similar conclusions were reached from analyses of the X-ray absorption near edge spectra (XANES) of Na^+ in solution.[45] Recent AIMD simulations carried out with the SCAN functional were found to accurately describe the hydration structure of Na^+ and K^+ in solution, although SCAN provided a relatively poorer description of liquid water.[46] Recent analyses have shown that the different performance of a given density functional in describing pure water and ions in water can be rationalized by considering the interplay between functional- and density-driven errors.[47–52]

Despite much progress in characterizing the hydration properties of ions in water, a transferable molecular model capable of correctly predicting structural, thermodynamic, and dynamical properties of hydrated ions from small aqueous clusters in the gas phase to aqueous solutions and interfaces is still missing. In the past years, we introduced the many-body energy (MB-nrg) theoretical/computational framework for data-driven many-body potential energy functions (PEFs).[53–56] The MB-nrg PEF of a molecular system is rigorously developed from the corresponding many-body expansion (MBE) of the system's energy that is generally calculated at the coupled cluster level of theory, including single, double, and perturbative triple excitations, i.e., CCSD(T), which is currently considered as the "gold standard" for chemical accuracy.[57] A series of MB-nrg PEFs developed for alkali-metal and halide ions was shown to accurately predict the structures, binding and interaction energies, and vibrational spectra of small $X^-(H_2O)_N$ (with X = F, Cl, Br, and I)[58–61] and $M^+(H_2O)_N$ (with M = Li, Na, K, Rb, and Cs) clusters as well as the hydration structures of Cl^-, Br^-, and I^- in solution.[62,63] In this study, we continue our analyses of the hydration properties of ions in solution by presenting the results of MD simulations carried out with the MB-nrg PEFs for single Na^+ and K^+ ions in solution.

METHODS

MB-nrg potential energy functions

The MB-nrg PEF of a N-monomer system is derived from the MBE which allows for rigorously calculating the system's energy, E_N, as the sum of individual terms representing the corresponding n-body energies, ϵ^{nB}, where $n \leq N$,[64]

$$E_N(1,..,N) = \sum_{i=1}^{N} \epsilon^{\mathrm{1B}}(i) + \sum_{i<j}^{N} \epsilon^{\mathrm{2B}}(i,j) + \sum_{i<j<k}^{N} \epsilon^{\mathrm{3B}}(i,j,k) + ... + \epsilon^{\mathrm{NB}}(1,..,N) \qquad (1)$$

In Eq. 1, ϵ^{1B} represents the 1-body (1B) energy corresponding to the distortion energy of an isolated monomer, and the remaining n-body energies ϵ^{nB} are calculated recursively using

$$\epsilon^{\mathrm{nB}} = E_n(1,...,n) - \sum_{i=1}^{N} \epsilon^{\mathrm{1B}}(i) - \sum_{i<j}^{N} \epsilon^{\mathrm{2B}}(i,j) - \sum_{i<j<k}^{N} \epsilon^{\mathrm{3B}}(i,j,k) - \ldots - \epsilon^{(\mathrm{n\text{-}1})\mathrm{B}}(1,2,3,...,n-1) \quad (2)$$

where E_n is the energy of a subsystem containing n monomers.

The MB-nrg PEFs for Na^+ and K^+ approximate Eq. 1 through an explicit sum of all 1B, 2B, and 3B terms which is supplemented with an implicit NB term representing classical N-body polarization derived from the corresponding TTM-nrg PEFs.[54] The functional form of the MB-nrg PEF is thus expressed as

$$E_N = \sum_{i=1}^{N} \epsilon^{\mathrm{1B}}(i) + \sum_{i>j}^{N} \epsilon^{\mathrm{2B}}(i,j) + \sum_{i>j>k}^{N} \epsilon^{\mathrm{3B}}(i,j,k) + V_{\mathrm{pol}} \qquad (3)$$

The 1B, 2B, and 3B terms that involve only the water molecules are described by the MB-pol PEF.[65–67] MB-pol has been shown to correctly reproduce the properties of water across all phases,[68,69] including gas-phase clusters[70–81] liquid water at ambient conditions[82–88] and in the supercooled regime,[89] the air/water interface,,[90–94] and various ice phases.[95–98] The 2B and 3B ion–water terms were fitted to reproduce the corresponding 2B and 3B reference energies that were calculated at the explicitly correlated coupled cluster and canonical cou-

pled cluster levels of theory, respectively, including single, double, and perturbative triple excitations, i.e., CCSD(T)-F12b for the 2-body energies, and CCSD(T) for the 3-body energies.[99,100]

The ion–water 2B terms of the MB-nrg PEFs were introduced in Ref. 54 and take the following form:

$$\epsilon^{2B} = V_{sr}^{2B} + V_{elec} + V_{disp} \tag{4}$$

Here, V_{sr}^{2B} is represented by a permutationally invariant polynomial (PIP), V_{PIP}^{2B},[101] which is smoothly switched to zero as the distance between the ion and the oxygen of the water molecule is larger than a predefined cutoff. The cutoff is is set to 6.5 Å for Na^+–H_2O and 7.0 Å for K^+–H_2O.[54] It has been shown that V_{PIP}^{2B} effectively recovers quantum-mechanical short-range 2B interactions (e.g., exchange-repulsion, charge transfer, and charge penetration) that arise from the overlap of the electron densities associated with the ion and the water molecule in a dimer.[102,103] V_{elec} describes permanent electrostatic interactions in the ion–water dimer between the positive (+1e) charge of the alkali-metal ion and the MB-pol

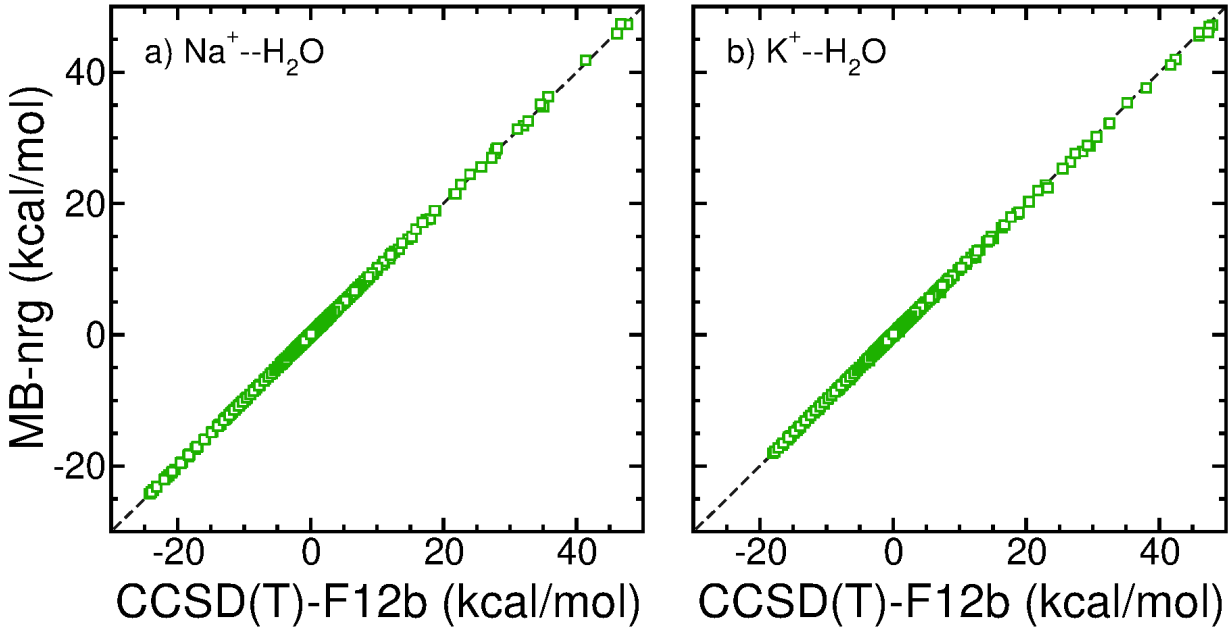

Figure 1: 2-body energy correlation plots between the CCSD(T)-F12b reference values (x-axis) and corresponding MB-nrg values (y-axis) for Na^+–H_2O (a) and K^+–H_2O (b).

geometry-dependent point charges of the water molecule.[65] The latter were fitted to reproduce the *ab initio* dipole moment of an isolated water molecule.[104] The last term in Eq. 4, $V_{\rm disp}$, describes the 2B dispersion energy.[54]

Fig. 1 shows the correlation between CCSD(T)-F12b and MB-nrg 2-body energies, which results in root-mean-square errors (RMSEs) of 0.072 kcal/mol and 0.105 kcal/mol for Na^+–H_2O and K^+–H_2O, respectively.

The ion–water–water 3B terms were derived following the same theoretical framework adopted in the development of analogous MB-nrg PEFs for Cs^+[105] and Cl^-.[62] Briefly, ϵ^{3B} is represented by a PIP, $V_{\rm PIP}^{3B}$,[101] that effectively describes 3B quantum-mechanical energy contributions that cannot be represented by classical polarization as well as short-range 3B dispersion energy contributions,

$$\epsilon^{3B} = [s_3(R_{M^+O_a})s_3(R_{M^+O_b}) + s_3(R_{M^+O_a})s_3(R_{O_aO_b}) + s_3(R_{M^+O_b})s_3(R_{O_aO_b})] \cdot V_{\rm PIP}^{3B} \qquad (5)$$

Here, $M^+ = Na^+$ or K^+, and s_3 is the same 3-body switching function used in Ref. 62 which depends on an inner ($R_{\rm in}^{3B}$) and an outer ($R_{\rm out}^{3B}$) cutoff distance. $R_{\rm in}^{3B}$ and $R_{\rm out}^{3B}$ were set to 0 Å and 4.5 Å, respectively, for both Na^+–H_2O–H_2O and K^+–H_2O–H_2O. $V_{\rm PIP}^{3B}$ is a function of all 21 pairwise distances between the physical atoms (H, O, and $M^+ = Na^+$, K^+) and the lone-pair sites of the two water molecules (L_1 and L_2) in a M^+–H_2O–H_2O trimer. $V_{\rm PIP}^{3B}$ contains 1016 symmetrized monomials: 13 second-degree monomials, 150 third-degree monomials, and 853 fourth-degree monomials.

The reference trimer configurations used in the parameterization of the M^+–H_2O–H_2O 3B energy terms were extracted from MD simulations carried out at ambient conditions in the isobaric-isothermal (NPT) ensemble using the (2B+NB)-MB-nrg PEFs of Ref. 54. The corresponding 3B energies were calculated at the CCSD(T) level of theory using the cc-pWCVTZ basis set[106–109] with counterpoise correction.[110] All CCSD(T) electronic structure calculations of the 3B energies were carried out using MOLPRO (version 2020.1).[111] $V_{\rm PIP}^{3B}$

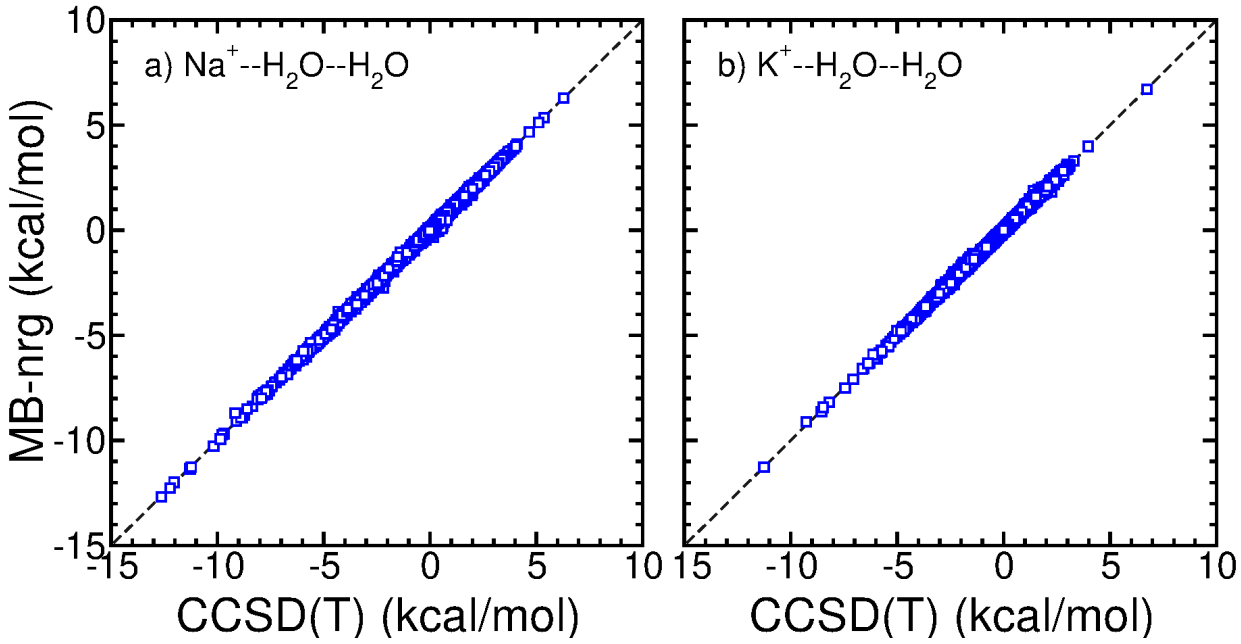

Figure 2: 3-body energy correlation plots between the CCSD(T) reference values (x-axis) and corresponding MB-nrg values (y-axis) for Na^+–H_2O–H_2O (a) and K^+–H_2O–H_2O (b).

was fitted following the same procedure adopted in the development of MB-pol[65,66] and other MB-nrg PEFs.[53–56,62,112] Specifically, we applied the ridge regression algorithm (also known as Tikhonov regularization),[113] where the linear parameters were optimized using singular value decomposition and the non-linear parameters were optimized using the simplex algorithm.

Fig. 2 shows that both MB-nrg PEFs are able to quantitatively reproduce the CCSD(T) 3B energies, resulting in RMSEs of 0.026 kcal/mol and 0.019 kcal/mol for Na^+–H_2O–H_2O and and K^+–H_2O–H_2O, respectively.

MD simulations and analysis

All MD simulations were carried out in the NPT ensemble at 298 K and 1.0 atm for a box containing a single ion and 277 water molecules, corresponding to an ionic solution of concentration of ∼0.2 M. The velocity-Verlet algorithm[114] with a timestep of 0.2 fs was used to propagate the equations of motion in the MD simulations with the TTM-nrg and MB-nrg PEFs, in which the induced dipole moments were propagated according to the always

stable predictor–corrector algorithm.[115] Nosé-Hoover chain thermostats of length 4 attached to each degree of freedom were used to control the temperature while the pressure was controlled using the algorithm described in Ref. 116. All MD simulations with the TTM-nrg and MB-nrg PEFs were carried out with an in-house version of DL_POLY 2.0.[117] For comparison, MD simulations were also carried out using the Na^+–H_2O and K^+–H_2O empirical parameterizations compatible with the TIP4P-Ew water model[118] which were introduced by Joung and Cheatham in Ref. 119. Hereafter, these force fields are labeled as JC+TIP4P-Ew. The JC+TIP4P-Ew simulations were carried out with LAMMPS[120] where the temperature and the pressure were maintained using a global Nosé–Hoover chain of 3 thermostats with a relaxation time of 1 ps, and a global Nosé–Hoover barostat with a relaxation time of 1 ps which was thermosttated by a Nosé–Hoove chain of three thermostats. After equilibration, all NPT simulations consisted of at least 1 ns of production. The TTM-nrg and MB-nrg PEFs used in this study are available in our open-access MBX software that can be downloaded from GitHub.[121]

The FEFF software was used to calculate the EXAFS spectra.[122–124] Following Refs. 125 and 62, all FEFF calculations were performed using clusters containing the alkali-metal ion and its 33 closest water molecules which were extracted from the corresponding MD trajectories at intervals of 0.5 ps.

RESULTS AND DISCUSSION

In Fig. 3 the experimental K-edge EXAFS spectra measured for Na^+ and K^+ in solution are compared with the corresponding spectra calculated with the JC+TIP4P-Ew force field, and the TTM-nrg, (2B+NB)-MB-nrg, and (2B+3B+NB)-MB-nrg PEFs. Appreciable differences exist among the four calculated spectra in the ability to reproduce both amplitudes and phases of the oscillations measured experimentally. Specifically, the JC+TIP4P-Ew force field overestimates the amplitude of the oscillations at all k. The agreement with the

experimental spectrum improves with the TTM-nrg PEF, which includes an implicit representation of many-body effects through classical polarization,[126] and becomes progressively quantitative upon including explicit representations of 2-body and 3-body interactions as implemented in the (2B+NB)-MB-nrg and (2B+3B+NB)-MB-nrg PEFs, respectively.

The differences found in the EXAFS spectra directly translate into different hydration structures as predicted by the JC+TIP4P-Ew force field, and the TTM-nrg, (2B+NB)-MB-nrg, and (2B+3B+NB)-MB-nrg PEFs for Na^+ and K^+ in solution. Fig. 4 compares the calculated M^+-O (panels a and c) and M^+-H (panels b and d) radial distribution functions (RDFs), with $M^+ = Na^+$ (top panels) and $M^+ = K^+$ (bottom panels), with the corresponding RDFs derived from neutron diffraction experiments.[127] In this regard, it should be noted that, since individual atom-atom RDFs cannot directly be extracted from neutron diffraction experiments, the experimentally-derived RDFs shown in Fig. 4 were obtained by using the empirical potential structure refinement (EPSR) method. In the EPSR process, empirical pairwise additive ion-water force fields were initially parameterized and used in combination with the SPC/E water model[128] to simulate the experimental diffraction patterns. The initial ion-water force fields were subsequently refined in an iterative way to improve the

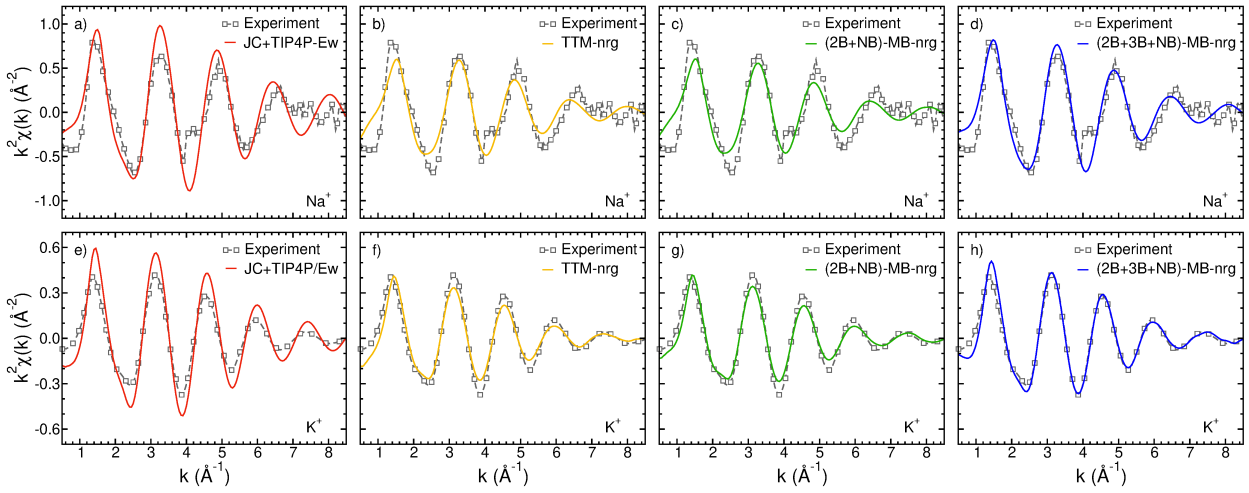

Figure 3: Comparisons among K-edge EXAFS spectra, $k^2\chi(k)$, of Na^+ (panels a-d) and K^+ (panels e-h) calculated from MD simulations with the JC+TIP4P-Ew force field, TTM-nrg, (2B+NB)-MB-nrg, and (2B+3B+NB)-MB-nrg PEFs. The experimental spectra are from Refs. 46.

agreement with the experimental data and then used to calculate all the atom-atom RDFs. The comparisons shown in Fig. 4 indicate that the larger oscillations observed in the EXAFS spectrum calculated with the JC+TIP4/Ew model are associated with more structured M^+-O and M^+-H RDFs. In contrast, the TTM-nrg and (2B+NB)-MB-nrg PEFs predict the least structured M^+-O RDFs, which is particularly evident in the case of K^+. The (2B+3B+NB)-MB-nrg PEFs predict M^+-O RDFs that are somewhat intermediate between those calculated with the JC+TIP4/Ew force fields and the TTM-nrg PEFs.

To summarize the results of the present MD simulations, Table 1 compares the first-shell

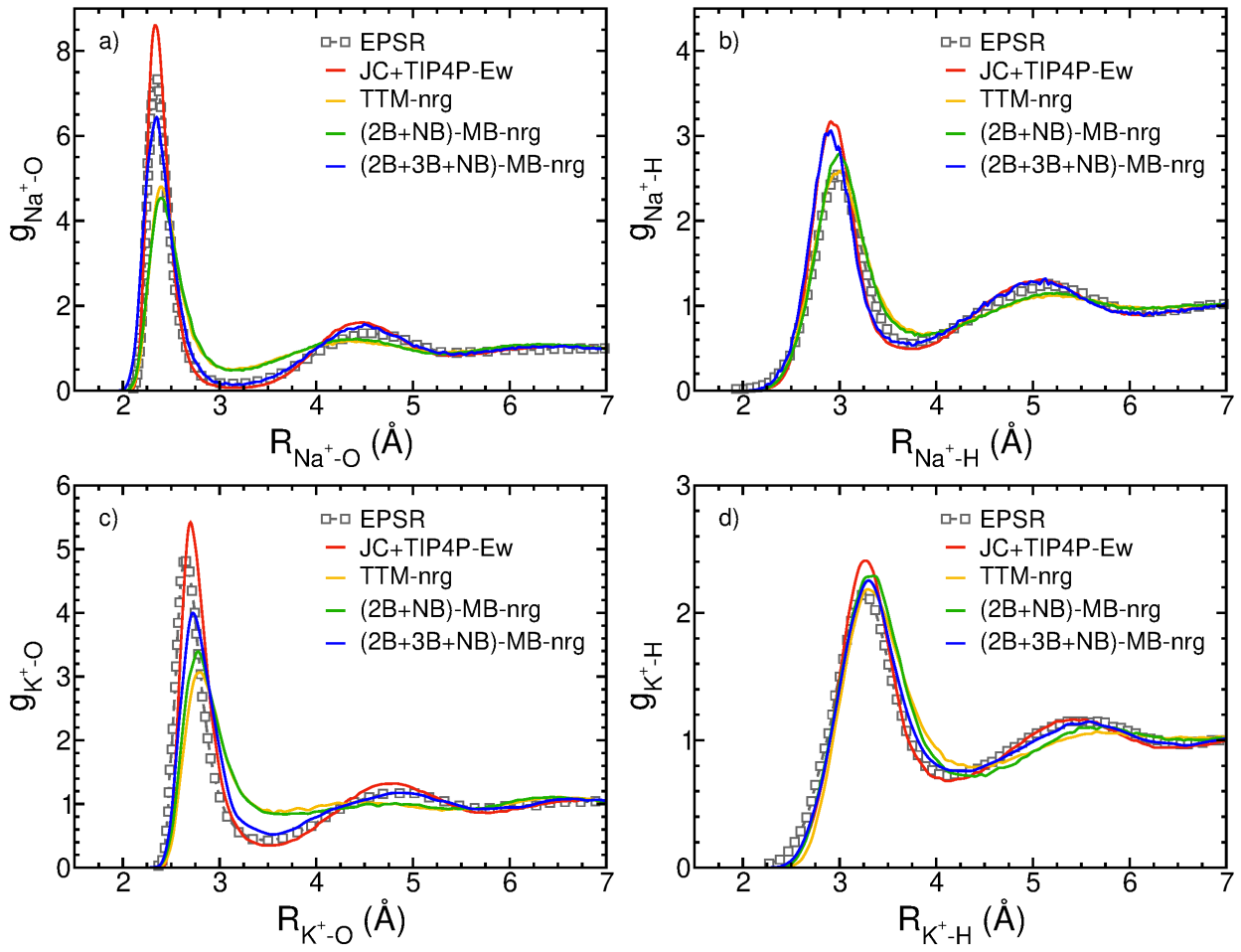

Figure 4: Top panels: Na^+–O (a) and Na^+–H (b) radial distribution functions calculated from MD simulations carried out with the JC+TIP4P-Ew force field, and the TTM-nrg, (2B+NB)-MB-nrg, and (2B+3B+NB)-MB-nrg PEFs. Bottom panels: Corresponding K^+–O (c) and K^+–H (d) radial distribution functions. The EPSR-based RDFs derived from neutron diffraction experiments are from Ref. 127.

Table 1: First-shell peak positions ($R_{\mathrm{O}}^{\mathrm{1st}}$) and coordination numbers ($\mathrm{CN}_{\mathrm{M^+-O}}$) derived from the Na^+–O and K^+–O RDFs calculated with the JC+TIP4P/Ew force field, and the TTM-nrg, (2B+NB)-MB-nrg, and (2B+3B+NB)-MB-nrg PEFs along with the corresponding experimental estimates determined from EXAFS,[44] X-ray diffraction,[44] and neutron diffraction measurements.[127]

model	$R_{\mathrm{O}}^{\mathrm{1st}}$	$\mathrm{CN}_{\mathrm{M^+-O}}$
Na^+		
JC+TIP4P-Ew	2.33	5.9
TTM-nrg	2.39	5.4
(2B+NB)-MB-nrg	2.39	5.4
(2B+3B+NB)-MB-nrg	2.35	5.8
EXAFS (6M NaCl)[44]	2.372(024)	5.4(1.3)
XRD (6M NaCl)[44]	2.384(003)	5.5(0.3)
XRD (2.5M NaCl)[44]	2.381(005)	5.9(0.6)
ND[127]	2.34	5
K^+		
JC+TIP4P-Ew	2.7	6.8
TTM-nrg	2.8	8.7
(2B+NB)-MB-nrg	2.8	7.7
(2B+3B+NB)-MB-nrg	2.7	6.7
ND[127]	2.7	6

peak positions ($R_{\mathrm{O}}^{\mathrm{1st}}$) and coordination numbers ($\mathrm{CN}_{\mathrm{M^+-O}}$) derived from the Na^+–O and K^+–O RDFs calculated with the JC+TIP4P/Ew force field, and the TTM-nrg, (2B+NB)-MB-nrg, and (2B+3B+NB)-MB-nrg PEFs with the corresponding experimental estimates determined from EXAFS,[44] X-ray diffraction,[44] and neutron diffraction measurements.[127]

Figs. 4a and 4c show that none of the four ion–water models analyzed in this study are able to reproduce the first peak of the EPSR-based Na^+-O and K^+-O RDFs derived from neutron diffraction measurements. In particular, the first peaks of the M^+-O and M^+-H RDFs calculated with the (2B+3B+NB)-MB-nrg PEFs, which provide the closest agreement with the experimental EXAFS spectra for both Na^+ and K^+ (Fig. 3), are respectively higher and lower than those predicted by the corresponding EPSR-based RDFs. Considering the sensitivity of the EXAFS measurements to the local structure of the first hydration shell and the difficulties in unambiguously separating individual atom-atom RDFs from neutron diffraction patterns, the agreement with the experimental EXAFS spectra provided by the

(2B+3B+NB)-MB-nrg PEF suggests that both the height and the position of the first peaks in the EPSR-based M^+-O and M^+-H RDFs may possibly need further refinement.

Additional insights into the local hydration structure of Na^+ and K^+ in solution is gained from the analysis of the incremental radial distribution functions (iRDFs) describing individual contributions to the corresponding M^+-O RDFs which are associated with each water molecule i as a function of its distance from the ion.[125] Following Ref. 44, each iRDF was fitted to a Gaussian function which allows for determining the location of the ith solvating water molecule in terms of the associated average distance from the ion, $\langle R_{M^+O_i} \rangle$, and variance of the Gaussian function, σ_i^2. The analyses of the Na^+-O_i and K^+-O_i iRDFs are shown in Figs. 5 and 6, respectively.

It is possible to qualitatively separate the four ion–water models in two subgroups, with one subgroup including the JC+TIP4P-Ew force field and the (2B+3B+NB)-MB-nrg PEF and the other group including the TTM-nrg and (2B+NB)-MB-nrg PEFs. In the case of Na^+, both the JC+TIP4P-Ew force field and the (2B+3B+NB)-MB-nrg PEF display a well-defined transition between the first and second hydration shells, which takes place

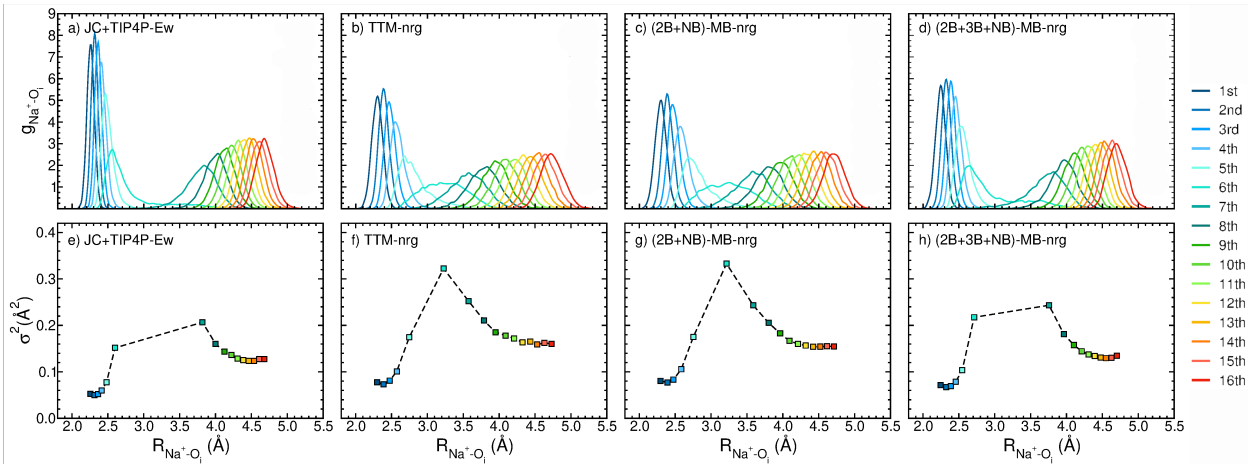

Figure 5: a-d) Na^+-O_i incremental radial distribution functions (iRDFs) for the first 16 water molecules around the Na^+ ion calculated from MD simulations with the JC+TIP4P-Ew force field, and the TTM-nrg, (2B+NB)-MB-nrg, and (2B+3B+NB)-MB-nrg PEFs. e-h) Average distances (x-axis) and variances (y-axis) associated with the Gaussian functions that were fitted to the iRDFs shown in the corresponding top panels. The same color scheme is used in the top and bottom panels.

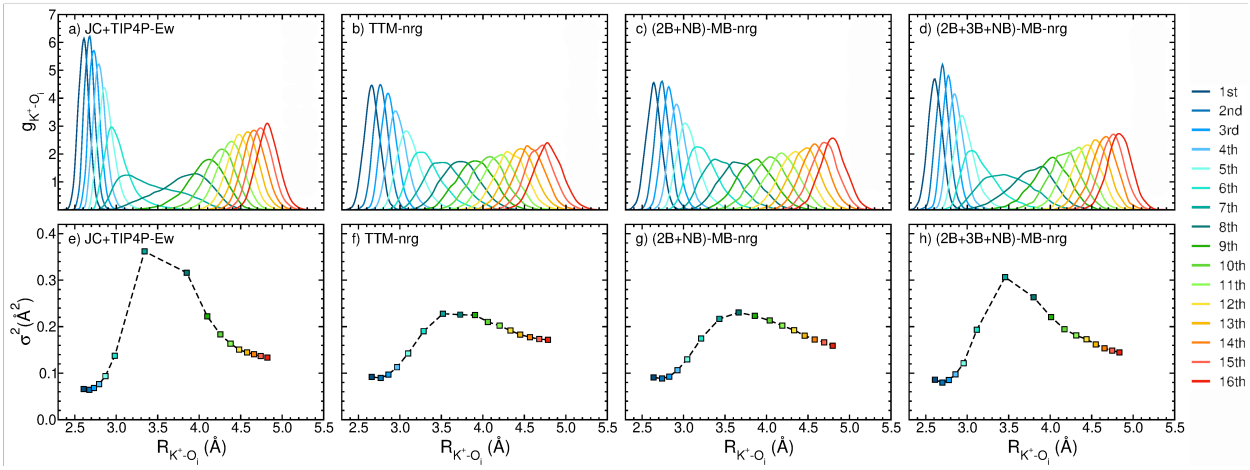

Figure 6: a-d) K^+-O_i incremental radial distribution functions (iRDFs) for the first 16 water molecules around the K^+ ion calculated from MD simulations with the JC+TIP4P-Ew, TTM-nrg, (2B+NB)-MB-nrg, and (2B+3B+NB)-MB-nrg models. e-h) Average distances (x-axis) and variances (y-axis) associated with the Gaussian functions that were fitted to the iRDFs shown in the corresponding top panels. The same color scheme was used in the top and bottom panels.

between the 6^{th} and the 7^{th} solvating water molecule. However, the JC+TIP4P-Ew force field predicts a more compact first hydration shell, which correlates with the overestimation of the amplitudes in the corresponding EXAFS spectrum. In contrast, the TTM-nrg and (2B+NB)-MB-nrg PEFs predict a softer first hydration shell, which is accompanied by a nearly continuous transition from the first to the second hydration shell. Although similar trends are also found in the iRDFs for K^+ in solution, in this case, the transition between the first and the second hydration shell is predicted to be less sharp by all models, including the JC+TIP4P-Ew force field and the (2B+3B+NB)-MB-nrg PEF which show significant overlap between the spatial distributions associated with the $7th$ and $8th$ solvating water molecules. The differences in the local hydration structure of Na^+ and K^+ in solution are directly related to differences in the underlying many-body interactions as discussed in Ref. 103.

To place the results obtained in this study in context, Fig. 7 shows comparisons between the Na^+-O and K^+-O RDFs calculated using the (2B+3B+NB)-MB-nrg PEF with the corresponding RDFs reported in the literature for various force fields and DFT mod-

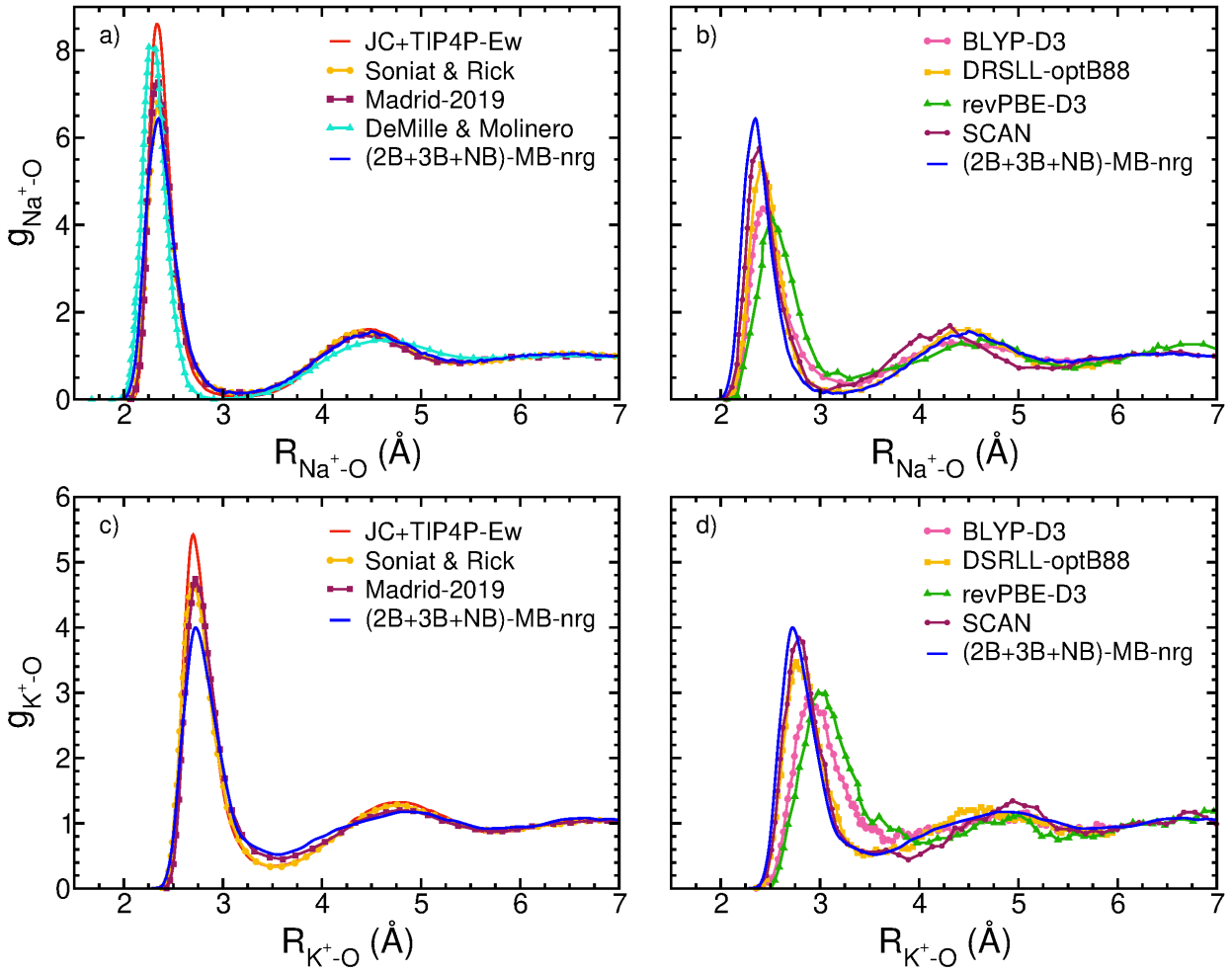

Figure 7: Comparisons between the Na^+–O (top panels) and K^+–O (bottom panels) radial distribution functions calculated from MD simulations carried out with the (2B+3B+NB)-MB-nrg PEF and the corresponding RDFs reported in literature for various force fields (panels a and c)[21,39,129] and DFT models (panels b and d).[33,46]

els. Interestingly, the force field and DFT predictions follow opposite trends relatively to the (2B+3B+NB)-MB-nrg PEF results, which effectively reflect the ability of the different models to better represent water–water and ion–water interactions. In particular, the force field proposed by Soniat and Rick, which includes charge transfer, as well as the Madrid-2019 force field, which empirically includes polarization effects and charge transfer through scaled atomic charges, predict lower first peaks compared to the JC+TIP4P-Ew force field, resulting in relatively closer agreement with the Na^+-O and K^+-O RDFs calculated with the (2B+3B+NB)-MB-nrg PEF. In contrast, the coarse-grained Na^+–H_2O model by DeMille

and Molinero, which is based on the single-site mW water model,[129] predicts a more structured first hydration shell similar to that obtained with the JC+TIP4P-Ew force field but shifted to shorter distances.

Regarding the DFT models, the simplest density functionals, such as BLYP-D3 and revPBE-D3, which were developed within the generalized gradient approximation (GGA), predict appreciably shallower first hydration shells that are shifted to larger distances (by ∼0.25 Å) compared to the RDFs calculated with the (2B+3B+NB)-MB-nrg PEF. In contrast, DRSLL-opt88, which was optimized for van der Waals and hydrogen-bonding interactions,[130] and SCAN, which is a nonempirical functional that satisfies all 17 constraints known for meta-GGA functionals,[131] predict a more structured first hydration shell that is shifted towards shorter distances, in better agreement with the (2B+3B+NB)-MB-nrg results. In this context, it should be noted that recent studies demonstrated that several density functionals suffer from both functional- and density-driven errors which significantly affect their performance when applied to aqueous systems.[47–52] In particular, large density-driven errors were found in SCAN calculations for pure water systems as well as for ions in water,[48,51,52] which suggests that the apparent agreement between the RDFs calculated from MD simulations with the SCAN functional and the (2B+3B+NB)-MB-nrg PEF may result from error cancellation in the SCAN representation of water–water and ion–water interactions.

CONCLUSIONS

In this study, we systematically characterized the hydration structure of Na^+ and K^+ ions in solution using a hierarchy of molecular models that differ in how they represent many-body effects in ion–water interactions. Our analyses demonstrate that, while the pairwise additive JC+TIP4P-Ew force field, which is commonly used in biosimulations, is able to qualitatively capture many-body effects through its empirical parameterization based on bulk properties, it does not provide a correct description of the local hydration structure of both Na^+ and

K^+ in solution. On the other hand, we found that the inclusion of classical polarization improves the description of many-body effects at intermediate and long ranges as shown by the closer agreement provided by the TTM-nrg models with the experimental EXAFS spectra compared to the JC+TIP4P-Ew force field. Our analyses show that progressive inclusion of explicit short-range 2-body and 3-body interactions as implemented in the MB-nrg PEFs is required to systematically improves the agreement with the experimental EXAFS spectra, which becomes nearly quantitative in the case of the (2B+3B+NB)-MB-nrg PEF. Importantly, the (2B+3B+NB)-MB-nrg PEFs predict hydration structures for both Na^+ and K^+ in solution which are distinct from those predicted by both the JC+TIP4P-Ew force field and the TTM-nrg PEF.

Comparisons with simulation results reported in the literature show that more recent empirical force fields, which either include an explicit charge transfer term or implicitly represent polarization effects and charge transfer through scaled atomic charges, are in relatively better agreement with the (2B+3B+NB)-MB-nrg PEF than the JC+TIP4P-Ew force field. On the other hand, GGA functionals, which are commonly used in AIMD simulations of aqueous systems, such as BLYP-D3 and revPBE-D3, provide a poor representation of the hydration structure of both Na^+ and K^+ in solution. More recent functionals, which were either optimized for van der Waals and hydrogen-bonding interactions, such as DRSLL-optB88, or rigorously derived to satisfy all the 17 constraints known for meta-GGA functionals, such as SCAN, are in closer agreement with the (2B+3B+NB)-MB-nrg PEFs.

Considering that the (2B+3B+NB)-MB-nrg PEFs were already shown to correctly predict isomeric equilibria and vibrational spectra of both $Na^+(H_2O)_N$ and $K^+(H_2O)_N$ clusters, the analyses presented in this study provide further evidence for the high accuracy and transferability of the (2B+3B+NB)-MB-nrg PEFs. Both accuracy and transferability are key to predictive computer simulations of ionic aqueous systems across different phases, which have thus far remained elusive due to inherent limitations of existing ion–water molecular models, including force fields and density functionals. Future work with the (2B+3B+NB)-MB-nrg

PEFs will focus on investigating the role of nuclear quantum effects on the hydration properties of both halide and alkali-metal ions as well as on characterizing single-ion free energies of hydration as well as structural, thermodynamic, and dynamical properties of ionic aqueous solutions as a function of their composition.

ACKNOWLEDGEMENT

This research was supported by the National Science Foundation through Grant No. CHE-1453204. The simulations used resources of the Extreme Science and Engineering Discovery Environment (XSEDE), which is supported by the National Science Foundation through Grant No. ACI-1053575, and the Triton Shared Computing Cluster (TSCC) at the San Diego Supercomputer Center.

References

(1) Marcus, Y. *Ion Solvation*; Wiley, 1985.

(2) Ussing, H. H.; Kruhoffer, P.; Thaysen, H. J.; Thorn, N. *The Alkali Metal Ions in Biology: I. The Alkali Metal Ions in Isolated Systems and Tissues. II. The Alkali Metal Ions in the Organism*; Springer Science & Business Media, 2013; Vol. 13.

(3) Guyton, A. C.; Hall, J. E., et al. *Textbook of Medical Physiology*; Saunders Philadelphia, 1986; Vol. 548.

(4) Wright, S. H. Generation of Resting Membrane Potential. *Adv. Physiol. Educ.* **2004**, *28*, 139–142.

(5) Feraille, E.; Doucet, A. Sodium-Potassium-Adenosinetriphosphatase-Dependent Sodium Transport in the Kidney: Hormonal Control. *Physiol. Rev.* **2001**, *81*, 345–418.

(6) Haddy, F.; Pamnani, M.; Clough, D. The Sodium-Potassium Pump in Volume Expanded Hypertension. *Clin. Exp. Hypertens.* **1978**, *1*, 295–336.

(7) Xie, Z.; Askari, A. Na+/K+-ATPase as a Signal Transducer. *Eur. J. Biochem.* **2002**, *269*, 2434–2439.

(8) Cressman, J. R.; Ullah, G.; Ziburkus, J.; Schiff, S. J.; Barreto, E. The Influence of Sodium and Potassium Dynamics on Excitability, Seizures, and the Stability of Persistent States: I. Single Neuron Dynamics. *J. Comput. Neurosci.* **2009**, *26*, 159–170.

(9) Ullah, G.; Cressman Jr, J. R.; Barreto, E.; Schiff, S. J. The Influence of Sodium and Potassium Dynamics on Excitability, Seizures, and the Stability of Persistent States: II. Network and Glial Dynamics. *J. Comput. Neurosci.* **2009**, *26*, 171–183.

(10) Hwang, J.-Y.; Myung, S.-T.; Sun, Y.-K. Sodium-Ion Batteries: Present and Future. *Chem. Soc. Rev.* **2017**, *46*, 3529–3614.

(11) Rajagopalan, R.; Tang, Y.; Ji, X.; Jia, C.; Wang, H. Advancements and Challenges in Potassium Ion Batteries: A Comprehensive Review. *Adv. Funct. Mater.* **2020**, *30*, 1909486.

(12) Borodin, O.; Bell, R. L.; Li, Y.; Bedrov, D.; Smith, G. D. Polarizable and Nonpolarizable Potentials for K^+ Cation in Water. *Chem. Phys. Lett.* **2001**, *336*, 292–302.

(13) Hartke, B.; Charvat, A.; Reich, M.; Abel, B. Experimental and Theoretical Investigation of Microsolvation of Na^+-Ions in the Gas Phase by High Resolution Mass Spectrometry and Global Cluster Geometry Optimization. *J. Chem. Phys.* **2002**, *116*, 3588–3600.

(14) Schulz, F.; Hartke, B. Dodecahedral Clathrate Structures and Magic Numbers in Alkali Cation Microhydration Clusters. *ChemPhysChem* **2002**, *3*, 98–106.

(15) Rao, J. S.; Dinadayalane, T.; Leszczynski, J.; Sastry, G. N. Comprehensive Study on the Solvation of Mono- and Divalent Metal Cations: Li^+, Na^+, K^+, Be^{2+}, Mg^{2+} and Ca^{2+}. *J. Phys. Chem. A* **2008**, *112*, 12944–12953.

(16) Ouni, O.; Derbel, N.; Jaïdane, N.; Ruiz-López, M. The K^+ Hydration Shell Structure in Non-Polar and Low-Polar Environments. *Comput. Theor. Chem.* **2012**, *990*, 209–213.

(17) Fifen, J. J.; Agmon, N. Ionic Radii of Hydrated Sodium Cation from QTAIM. *J. Chem. Phys.* **2019**, *150*, 034304.

(18) Migliore, M.; Corongiu, G.; Clementi, E.; Lie, G. Monte Carlo Study of Free Energy of Hydration for Li^+, Na^+, K^+, F^-, and Cl^- with Ab Initio Potentials. *J. Chem. Phys.* **1988**, *88*, 7766–7771.

(19) Hummer, G.; Pratt, L. R.; Garcia, A. E. Free Energy of Ionic Hydration. *J. Phys. Chem.* **1996**, *100*, 1206–1215.

(20) Grossfield, A.; Ren, P.; Ponder, J. W. Ion Solvation Thermodynamics from Simulation with a Polarizable Force Field. *J. Am. Chem. Soc.* **2003**, *125*, 15671–15682.

(21) Soniat, M.; Rick, S. W. The Effects of Charge Transfer on the Aqueous Solvation of Ions. *J. Chem. Phys.* **2012**, *137*, 044511.

(22) Öhrn, A.; Karlström, G. A Combined Quantum Chemical Statistical Mechanical Simulation of the Hydration of Li^+, Na^+, F^-, and Cl^-. *J. Phys. Chem. B* **2004**, *108*, 8452–8459.

(23) Tongraar, A.; Liedl, K. R.; Rode, B. M. Born-Oppenheimer Ab Initio QM/MM Dynamics Simulations of Na^+ and K^+ in Water: From Structure Making to Structure Breaking Effects. *J. Phys. Chem. A* **1998**, *102*, 10340–10347.

(24) Tongraar, A.; Rode, B. M. Dynamical Properties of Water Molecules in the Hydration Shells of Na^+ and K^+: Ab Initio QM/MM Molecular Dynamics Simulations. *Chem. Phys. Lett.* **2004**, *385*, 378–383.

(25) Rempe, S. B.; Pratt, L. R. The Hydration Number of Na^+ in Liquid Water. *Fluid Phase Equilib.* **2001**, *183*, 121–132.

(26) Rempe, S. B.; Asthagiri, D.; Pratt, L. R. Inner Shell Definition and Absolute Hydration Free Energy of K^+(aq) on the Basis of Quasi-Chemical Theory and Ab Initio Molecular Dynamics. *Phys. Chem. Chem. Phys.* **2004**, *6*, 1966–1969.

(27) Whitfield, T. W.; Varma, S.; Harder, E.; Lamoureux, G.; Rempe, S. B.; Roux, B. Theoretical Study of Aqueous Solvation of K^+ Comparing Ab Initio, Polarizable, and Fixed-Charge Models. *J. Chem. Theory Comput.* **2007**, *3*, 2068–2082.

(28) Bucher, D.; Kuyucak, S. Polarization of Water in the First Hydration Shell of K^+ and Ca^{2+} Ions. *J. Phys. Chem. B* **2008**, *112*, 10786–10790.

(29) Rey, R.; Hynes, J. T. Hydration Shell Exchange Kinetics: An MD Study for Na^+(aq). *J. Phys. Chem.* **1996**, *100*, 5611–5615.

(30) Degrève, L.; Vechi, S. M.; Junior, C. Q. The Hdration Structure of the Na^+ and K^+ Ions and the Selectivity of their Ionic Channels. *Biochim. Biophys. Acta Bioenerg.* **1996**, *1274*, 149–156.

(31) Faginas-Lago, N.; Lombardi, A.; Albertí, M.; Grossi, G. Accurate Analytic Intermolecular Potential for the Simulation of Na^+ and K^+ Ion Hydration in Liquid Water. *J. Mol. Liq.* **2015**, *204*, 192–197.

(32) Liu, Y.; Lu, H.; Wu, Y.; Hu, T.; Li, Q. Hydration and Coordination of K^+ Solvation in Water from Ab Initio Molecular-Dynamics Simulation. *J. Chem. Phys.* **2010**, *132*, 124503.

(33) Bankura, A.; Carnevale, V.; Klein, M. L. Hydration Structure of Na^+ and K^+ from Ab Initio Molecular Dynamics Based on Modern Density Functional Theory. *Mol. Phys.* **2014**, *112*, 1448–1456.

(34) Wanprakhon, S.; Tongraar, A.; Kerdcharoen, T. Hydration Structure and Dynamics of K^+ and Ca^{2+} in Aqueous Solution: Comparison of Conventional QM/MM and ONIOM-XS MD Simulations. *Chem. Phys. Lett.* **2011**, *517*, 171–175.

(35) Rowley, C. N.; Roux, B. The Solvation Structure of Na^+ and K^+ in Liquid Water Determined from High Level Ab Initio Molecular Dynamics Simulations. *J. Chem. Theory Comput.* **2012**, *8*, 3526–3535.

(36) Ma, H. Hydration Structure of Na^+, K^+, F^-, and Cl^- in Ambient and Supercritical Water: A Quantum Mechanics/Molecular Mechanics Study. *Int. J. Quantum Chem.* **2014**, *114*, 1006–1011.

(37) Kohagen, M.; Mason, P. E.; Jungwirth, P. Accounting for Electronic Polarization Effects in Aqueous Sodium Chloride Via Molecular Dynamics Aided by Neutron Scattering. *J. Phys. Chem. B* **2016**, *120*, 1454–1460.

(38) Mason, P. E.; Wernersson, E.; Jungwirth, P. Accurate Description of Aqueous Carbonate Ions: An Effective Polarization Model Verified by Neutron Scattering. *J. Phys. Chem. B* **2012**, *116*, 8145–8153.

(39) Zeron, I.; Abascal, J.; Vega, C. A force field of Li^+, Na^+, K^+, Mg^{2+}, Ca^{2+}, Cl^-, and SO_4^{2-} in Aqueous Solution Based on the TIP4P/2005 Water Model and Scaled Charges for the Ions. *J. Chem. Phys.* **2019**, *151*, 134504.

(40) Loche, P.; Steinbrunner, P.; Friedowitz, S.; Netz, R. R.; Bonthuis, D. J. Transferable Ion Force Fields in Water from a Simultaneous Optimization of Ion Solvation and Ion–Ion Interaction. *J. Phys. Chem. B* **2021**, *125*, 8581–8587.

(41) Dočkal, J.; Lísal, M.; Moučka, F. Polarizable Force Fields for Accurate Molecular Simulations of Aqueous Solutions of Electrolytes, Crystalline Salts, and Solubility: Li^+, Na^+, K^+, Rb^+, F^-, Cl^-, Br^-, I^-. *J. Mol. Liq.* **2022**, 119659.

(42) Glezakou, V.-A.; Chen, Y.; Fulton, J. L.; Schenter, G. K.; Dang, L. X. Electronic Structure, Statistical Mechanical Simulations, and EXAFS Spectroscopy of Aqueous Potassium. *Theor. Chem. Acc.* **2006**, *115*, 86–99.

(43) Dang, L. X.; Schenter, G. K.; Glezakou, V.-A.; Fulton, J. L. Molecular Simulation Analysis and X-ray Absorption Measurement of Ca^{2+}, K^+ and Cl^- Ions in Solution. *J. Phys. Chem. B* **2006**, *110*, 23644–23654.

(44) Galib, M.; Baer, M.; Skinner, L.; Mundy, C.; Huthwelker, T.; Schenter, G.; Benmore, C.; Govind, N.; Fulton, J. L. Revisiting the Hydration Structure of Aqueous Na^+. *J. Chem. Phys.* **2017**, *146*, 084504.

(45) Galib, M.; Schenter, G.; Mundy, C.; Govind, N.; Fulton, J. Unraveling the Spectral Signatures of Solvent Ordering in K-edge XANES of Aqueous Na^+. *J. Chem. Phys.* **2018**, *149*, 124503.

(46) Duignan, T. T.; Schenter, G. K.; Fulton, J. L.; Huthwelker, T.; Balasubramanian, M.; Galib, M.; Baer, M. D.; Wilhelm, J.; Hutter, J.; Del Ben, M., et al. Quantifying the Hydration Structure of Sodium and Potassium Ions: Taking Additional Steps on Jacob's Ladder. *Phys. Chem. Chem. Phys.* **2020**, *22*, 10641–10652.

(47) Vuckovic, S.; Song, S.; Kozlowski, J.; Sim, E.; Burke, K. Density Functional Analysis: The Theory of Density-Corrected DFT. *J. Chem. Theory Comput.* **2019**, *15*, 6636–6646.

(48) Dasgupta, S.; Lambros, E.; Perdew, J. P.; Paesani, F. Elevating Density Functional Theory to Chemical Accuracy for Water Simulations through a Density-Corrected Many-Body Formalism. *Nat. Commun.* **2021**, *12*, 1–12.

(49) Song, S.; Vuckovic, S.; Sim, E.; Burke, K. Density-Corrected DFT Explained: Questions and Answers. *J. Chem. Theory Comput.* **2022**, *18*, 817–827.

(50) Sim, E.; Song, S.; Vuckovic, S.; Burke, K. Improving Results by Improving Densities: Density-Corrected Density Functional Theory. *J. Am. Chem. Soc.* **2022**, *144*, 6625–6639.

(51) Palos, E.; Lambros, E.; Swee, S.; Hu, J.; Dasgupta, S.; Paesani, F. Assessing the Interplay Between Functional-Driven and Density-Driven Errors in DFT Models of Water. *J. Chem. Theory Comput.* **2022**, *18*, 3410–3426.

(52) Dasgupta, S.; Shahi, C.; Bhetwal, P.; Perdew, J. P.; Paesani, F. How Good Is the Density-Corrected SCAN Functional for Neutral and Ionic Aqueous Systems, and What Is So Right about the Hartree–Fock Density? *J. Chem. Theory Comput.* **2022**, *18*, 4745–4761.

(53) Bajaj, P.; Götz, A. W.; Paesani, F. Toward Chemical Accuracy in the Description of Ion–Water Interactions Through Many-Body Representations. I. Halide–Water Dimer Potential Energy Surfaces. *J. Chem. Theory. Comput.* **2016**, *12*, 2698–2705.

(54) Riera, M.; Mardirossian, N.; Bajaj, P.; Götz, A. W.; Paesani, F. Toward Chemical Accuracy in the Description of Ion–Water Interactions Through Many-Body Representations. Alkali-Water Dimer Potential Energy Surfaces. *J. Chem. Phys.* **2017**, *147*, 161715.

(55) Riera, M.; Yeh, E. P.; Paesani, F. Data-Driven Many-Body Models for Molecular Fluids: CO_2/H_2O Mixtures as a Case Study. *J. Chem. Theory. Comput.* **2020**, *16*, 2246–2257.

(56) Riera, M.; Hirales, A.; Ghosh, R.; Paesani, F. Data-Driven Many-Body Models with Chemical Accuracy for CH_4/H_2O Mixtures. *J. Phys. Chem. B* **2020**, *124*, 11207–11221.

(57) Rezac, J.; Hobza, P. Benchmark Calculations of Interaction Energies in Noncovalent Complexes and their Applications. *Chem. Rev.* **2016**, *116*, 5038–5071.

(58) Bajaj, P.; Wang, X.-G.; CarringtonJr, T.; Paesani, F. Vibrational Spectra of Halide-Water Dimers: Insights on Ion Hydration from Full-Dimensional Quantum Calculations on Many-Body Potential Energy Surfaces. *J. Chem. Phys.* **2017**, *148*, 102321.

(59) Bajaj, P.; Zhuang, D.; Paesani, F. Specific Ion Effects on Hydrogen-Bond Rearrangements in the Halide–Dihydrate Complexes. *J. Phys. Chem. Lett.* **2019**, *10*, 2823–2828.

(60) Bajaj, P.; Riera, M.; Lin, J. K.; Mendoza Montijo, Y. E.; Gazca, J.; Paesani, F. Halide Ion Microhydration: Structure, Energetics, and Spectroscopy of Small Halide–Water Clusters. *J. Phys. Chem. A* **2019**, *123*, 2843–2852.

(61) Paesani, F.; Bajaj, P.; Riera, M. Chemical Accuracy in Modeling Halide Ion Hydration from Many-Body Representations. *Adv. Phys. X* **2019**, *4*, 1631212.

(62) Caruso, A.; Paesani, F. Data-Driven Many-Body Models Enable a Quantitative Description of Chloride Hydration from Clusters to Bulk. *J. Chem. Phys.* **2021**, *155*, 064502.

(63) Caruso, A.; Zhu, X.; Paesani, F. Accurate Modeling of Bromide and Iodide Hydration with Data-Driven Many-Body Potentials. *J. Phys. Chem. B* **2022**, in press, https://doi.org/10.1021/acs.jpcb.2c04698.

(64) Nesbet, R. Atomic Bethe-Goldstone Equations. *Adv. Chem. Phys.* **1969**, 1–34.

(65) Babin, V.; Leforestier, C.; Paesani, F. Development of a "First Principles" Water Potential With Flexible Monomers: Dimer Potential Energy Surface, VRT Spectrum, and Second Virial Coefficient. *J. Chem. Theory. Comput.* **2013**, *9*, 5395–5403.

(66) Babin, V.; Medders, G. R.; Paesani, F. Development of a "First Principles" Water

Potential With Flexible Monomers. II: Trimer Potential Energy Surface, Third Virial Coefficient, and Small Clusters. *J. Chem. Theory. Comput.* **2014**, *10*, 1599–1607.

(67) Medders, G. R.; Babin, V.; Paesani, F. Development of a "First Principles" Water Potential With Flexible Monomers. III. Liquid Phase Properties. *J. Chem. Theory. Comput.* **2014**, *10*, 2906–2910.

(68) Reddy, S. K.; Straight, S. C.; Bajaj, P.; Huy Pham, C.; Riera, M.; Moberg, D. R.; Morales, M. A.; Knight, C.; Götz, A. W.; Paesani, F. On the Accuracy of the MB-pol Many-Body Potential for Water: Interaction Energies, Vibrational Frequencies, and Classical Thermodynamic and Dynamical Properties from Clusters to Liquid water and Ice. *J. Chem. Phys.* **2016**, *145*, 194504.

(69) Paesani, F. Getting the Right Answers for the Right Reasons: Toward Predictive Molecular Simulations of Water With Many-Body Potential Energy Functions. *Acc. Chem. Res.* **2016**, *49*, 1844–1851.

(70) Richardson, J. O.; Pérez, C.; Lobsiger, S.; Reid, A. A.; Temelso, B.; Shields, G. C.; Kisiel, Z.; Wales, D. J.; Pate, B. H.; Althorpe, S. C. Concerted Hydrogen-Bond Breaking by Quantum Tunneling in the Water Hexamer Prism. *Science* **2016**, *351*, 1310–1313.

(71) Cole, W. T.; Farrell, J. D.; Wales, D. J.; Saykally, R. J. Structure and Torsional Dynamics of the Water Octamer from THz Laser Spectroscopy Near 215 μm. *Science* **2016**, *352*, 1194–1197.

(72) Mallory, J. D.; Mandelshtam, V. A. Diffusion Monte Carlo Studies of MB-pol $(H_2O)_{2-6}$ and $(D_2O)_{2-6}$ clusters: Structures and Binding Energies. *J. Chem. Phys.* **2016**, *145*, 064308.

(73) Videla, P. E.; Rossky, P. J.; Laria, D. Communication: Isotopic Effects on Tunneling Motions in the Water Trimer. *J. Chem. Phys.* **2016**, *144*, 061101.

(74) Brown, S. E.; Götz, A. W.; Cheng, X.; Steele, R. P.; Mandelshtam, V. A.; Paesani, F. Monitoring Water Clusters "Melt" through Vibrational Spectroscopy. *J. Am. Chem. Soc.* **2017**, *139*, 7082–7088.

(75) Vaillant, C. L.; Cvitaš, M. T. Rotation-Tunneling Spectrum of the Water Dimer from Instanton Theory. *Phys. Chem. Chem. Phys.* **2018**, *20*, 26809–26813.

(76) Vaillant, C.; Wales, D.; Althorpe, S. Tunneling Splittings from Path-Integral Molecular Dynamics Using a Langevin Thermostat. *J. Chem. Phys.* **2018**, *148*, 234102.

(77) Schmidt, M.; Roy, P.-N. Path Integral Molecular Dynamic Simulation of Flexible Molecular Systems in Their Ground State: Application to the Water Dimer. *J. Chem. Phys.* **2018**, *148*, 124116.

(78) Bishop, K. P.; Roy, P.-N. Quantum Mechanical Free Energy Profiles with Post-Quantization Restraints: Binding Free Energy of the Water Dimer Over a Broad Range of Temperatures. *J. Chem. Phys.* **2018**, *148*, 102303.

(79) Videla, P. E.; Rossky, P. J.; Laria, D. Isotopic Equilibria in Aqueous Clusters at Low Temperatures: Insights from the MB-pol Many-Body Potential. *J. Chem. Phys.* **2018**, *148*, 084303.

(80) Samala, N. R.; Agmon, N. Temperature Dependence of Intramolecular Vibrational Bands in Small Water Clusters. *J. Phys. Chem. B* **2019**, *123*, 9428–9442.

(81) Cvitaš, M. T.; Richardson, J. O. Quantum Tunnelling Pathways of the Water Pentamer. *Phys. Chem. Chem. Phys.* **2020**, *22*, 1035–1044.

(82) Medders, G. R.; Paesani, F. Infrared and Raman Spectroscopy of Liquid Water Through "First-Principles" Many-Body Molecular Dynamics. *J. Chem. Theory Comput.* **2015**, *11*, 1145–1154.

(83) Straight, S. C.; Paesani, F. Exploring Electrostatic Effects on the Hydrogen Bond Network of Liquid Water Through Many-Body Molecular Dynamics. *J. Phys. Chem. B* **2016**, *120*, 8539–8546.

(84) Reddy, S. K.; Moberg, D. R.; Straight, S. C.; Paesani, F. Temperature-Dependent Vibrational Spectra and Structure of Liquid Water from Classical and Quantum Simulations With the MB-pol Potential Energy Function. *J. Chem. Phys.* **2017**, *147*, 244504.

(85) Hunter, K. M.; Shakib, F. A.; Paesani, F. Disentangling Coupling Effects in the Infrared Spectra of Liquid Water. *J. Phys. Chem. B* **2018**, *122*, 10754–10761.

(86) Sun, Z.; Zheng, L.; Chen, M.; Klein, M. L.; Paesani, F.; Wu, X. Electron-Hole Theory of the Effect of Quantum Nuclei on the X-ray Absorption Spectra of Liquid Water. *Phys. Rev. Lett.* **2018**, *121*, 137401.

(87) Gaiduk, A. P.; Pham, T. A.; Govoni, M.; Paesani, F.; Galli, G. Electron Affinity of Liquid Water. *Nat. Commun.* **2018**, *9*, 1–6.

(88) Cruzeiro, V.; Wildman, A.; Li, X.; Paesani, F. Relationship Between Hydrogen-Bonding Motifs and the $1b_1$ Splitting in the X-ray Emission Spectrum of Liquid Water. *J. Phys. Chem. Lett.* **2021**, *12*, 3996–4002.

(89) Gartner III, T. E.; Hunter, K. M.; Lambros, E.; Caruso, A.; Riera, M.; Medders, G. R.; Panagiotopoulos, A. Z.; Debenedetti, P. G.; Paesani, F. Anomalies and Local Structure of Liquid Water from Boiling to the Supercooled Regime as Predicted by the Many-Body MB-pol Model. *J. Phys. Chem. Lett. 13*, 3652–3658.

(90) Medders, G. R.; Paesani, F. Dissecting the Molecular Structure of the Air/Water Interface from Quantum Simulations of the Sum-Frequency Generation Spectrum. *J. Am. Chem. Soc.* **2016**, *138*, 3912–3919.

(91) Moberg, D. R.; Straight, S. C.; Paesani, F. Temperature Dependence of the Air/Water Interface Revealed by Polarization Sensitive Sum-Frequency Generation Spectroscopy. *J. Phys. Chem. B* **2018**, *122*, 4356–4365.

(92) Sun, S.; Tang, F.; Imoto, S.; Moberg, D. R.; Ohto, T.; Paesani, F.; Bonn, M.; Backus, E. H.; Nagata, Y. Orientational Distribution of Free OH Groups of Interfacial Water is Exponential. *Phys. Rev. Lett.* **2018**, *121*, 246101.

(93) Sengupta, S.; Moberg, D. R.; Paesani, F.; Tyrode, E. Neat Water–Vapor Interface: Proton Continuum and the Nonresonant Background. *J. Phys. Chem. Lett.* **2018**, *9*, 6744–6749.

(94) Muniz, M. C.; Gartner III, T. E.; Riera, M.; Knight, C.; Yue, S.; Paesani, F.; Panagiotopoulos, A. Z. Vapor-Liquid Equilibrium of Water With the MB-pol Many-Body Potential. *J. Chem. Phys.* **2021**, *154*, 211103.

(95) Pham, C. H.; Reddy, S. K.; Chen, K.; Knight, C.; Paesani, F. Many-Body Interactions in Ice. *J. Chem. Theory Comput.* **2017**, *13*, 1778–1784.

(96) Moberg, D. R.; Straight, S. C.; Knight, C.; Paesani, F. Molecular Origin of the Vibrational Structure of Ice I_h. *J. Phys. Chem. Lett.* **2017**, *8*, 2579–2583.

(97) Moberg, D. R.; Sharp, P. J.; Paesani, F. Molecular-Level Interpretation of Vibrational Spectra of Ordered Ice Phases. *J. Phys. Chem. B* **2018**, *122*, 10572–10581.

(98) Moberg, D. R.; Becker, D.; Dierking, C. W.; Zurheide, F.; Bandow, B.; Buck, U.; Hudait, A.; Molinero, V.; Paesani, F.; Zeuch, T. The End of Ice I. *Proc. Natl. Acad. Sci. U.S.A.* **2019**, *116*, 24413–24419.

(99) Adler, T.; Knizia, G.; Werner, H. A Simple and Efficient CCSD(T)-F12 Approximation. *J. Chem. Phys.* **2007**, *127*, 221106–221106.

(100) Knizia, G.; Adler, T. B.; Werner, H.-J. Simplified CCSD(T)-F12 Methods: Theory and Benchmarks. *J. Chem. Phys.* **2009**, *130*, 054104.

(101) Braams, B. J.; Bowman, J. M. Permutationally Invariant Potential Energy Surfaces in High Dimensionality. *Int. Rev. Phys. Chem.* **2009**, *28*, 577–606.

(102) Bizzarro, B. B.; Egan, C. K.; Paesani, F. Nature of Halide–Water Interactions: Insights From Many-Body Representations and Density Functional Theory. *J. Chem. Theory. Comput.* **2019**, *15*, 2983–2995.

(103) Egan, C. K.; Bizzarro, B. B.; Riera, M.; Paesani, F. Nature of Alkali Ion–Water Interactions: Insights From Many-Body Representations and Density Functional Theory. II. *J. Chem. Theory. Comput.* **2020**, *16*, 3055–3072.

(104) Partridge, H.; Schwenke, D. W. The Determination of an Accurate Isotope Dependent Potential Energy Surface for Water From Extensive Ab Initio Calculations and Experimental Data. *J. Chem. Phys.* **1997**, *106*, 4618–4639.

(105) Riera, M.; Talbot, J. J.; Steele, R. P.; Paesani, F. Infrared Signatures of Isomer Selectivity and Symmetry Breaking in the $Cs^+(H_2O)_3$ Complex Using Many-Body Potential Energy Functions. *J. Chem. Phys.* **2020**, *153*, 044306.

(106) Pritchard, B. P.; Altarawy, D.; Didier, B.; Gibson, T. D.; Windus, T. L. New Basis Set Exchange: An Open, Up-to-Date Resource for the Molecular Sciences Community. *J. Chem. Inf. Model.* **2019**, *59*, 4814–4820.

(107) Dunning Jr, T. H. Gaussian Basis Sets for Use in Correlated Molecular Calculations. I. The Atoms Boron through Neon and Hydrogen. *J. Chem. Phys.* **1989**, *90*, 1007–1023.

(108) Kendall, R. A.; Dunning Jr, T. H.; Harrison, R. J. Electron Affinities of the First-Row Atoms Revisited. Systematic Basis Sets and Wave Functions. *J. Chem. Phys.* **1992**, *96*, 6796–6806.

(109) Woon, D. E.; Dunning Jr, T. H. Gaussian Basis Sets for Use in Correlated Molecular Calculations. III. The Atoms Aluminum through Argon. *J. Chem. Phys.* **1993**, *98*, 1358–1371.

(110) Boys, S. F.; Bernardi, F. The Calculation of Small Molecular Interactions by the Differences of Separate Total Energies. Some Procedures with Reduced Errors. *Mol. Phys.* **1970**, *19*, 553–566.

(111) Werner, H.-J.; Knowles, P. J.; Knizia, G.; Manby, F. R.; Schütz, M. Molpro: A General-Purpose Quantum Chemistry Program Package. *Wiley Interdiscip. Rev. Comput. Mol. Sci.* **2012**, *2*, 242–253.

(112) Cruzeiro, V. W. D.; Lambros, E.; Riera, M.; Roy, R.; Paesani, F.; Götz, A. W. Highly Accurate Many-Body Potentials for Simulations of N_2O_5 in Water: Benchmarks, Development, and Validation. *J. Chem. Theory Comput.* **2021**, *17*, 3931–3945.

(113) Hastie, T.; Tibshirani, R.; Friedman, J. *The Elements of Statistical Learning: Data Mining, Inference, and Prediction*; Springer Science & Business Media, 2009.

(114) Tuckerman, M.; Berne, B. J.; Martyna, G. J. Reversible Multiple Time Scale Molecular Dynamics. *J. Chem. Phys.* **1992**, *97*, 1990–2001.

(115) Kolafa, J. Time-Reversible Always Stable Predictor–Corrector Method for Molecular Dynamics of Polarizable Molecules. *J. Comp. Chem.* **2004**, *25*, 335–342.

(116) Martyna, G. J.; Klein, M. L.; Tuckerman, M. Nosé–Hoover Chains: The Canonical Ensemble Via Continuous Dynamics. *J. Chem. Phys.* **1992**, *97*, 2635–2643.

(117) Smith, W.; Forester, T. DL_POLY_2. 0: A General-Purpose Parallel Molecular Dynamics Simulation Package. *J. Mol. Graph.* **1996**, *14*, 136–141.

(118) Horn, H. W.; Swope, W. C.; Pitera, J. W.; Madura, J. D.; Dick, T. J.; Hura, G. L.;

Head-Gordon, T. Development of an Improved Four-Site Water Model for Biomolecular Simulations: TIP4P-Ew. *J. Chem. Phys.* **2004**, *120*, 9665–9678.

(119) Joung, I. S.; Cheatham III, T. E. Determination of Alkali and Halide Monovalent Ion Parameters for Use in Explicitly Solvated Biomolecular Simulations. *J. Phys. Chem. B* **2008**, *112*, 9020–9041.

(120) Thompson, A. P.; Aktulga, H. M.; Berger, R.; Bolintineanu, D. S.; Brown, W. M.; Crozier, P. S.; in 't Veld, P. J.; Kohlmeyer, A.; Moore, S. G.; Nguyen, T. D.; Shan, R.; Stevens, M. J.; Tranchida, J.; Trott, C.; Plimpton, S. J. LAMMPS - A Flexible Simulation Tool for Particle-Based Materials Modeling at the Atomic, Meso, and Continuum Scales. *Comput. Phys. Commun.* **2022**, *271*, 108171.

(121) MBX: A Many-Body Energy and Force Calculator. `https://github.com/paesanilab/MBX`.

(122) Rehr, J. J.; Kas, J. J.; Vila, F. D.; Prange, M. P.; Jorissen, K. Parameter-Free Calculations of X-Ray Spectra with FEFF9. *Phys. Chem. Chem. Phys.* **2010**, *12*, 5503–5513.

(123) Rehr, J. J.; Kas, J. J.; Prange, M. P.; Sorini, A. P.; Takimoto, Y.; Vila, F. Ab Initio Theory and Calculations of X-Ray Spectra. *C. R. Phys.* **2009**, *10*, 548–559.

(124) Rehr, J. J.; Albers, R. C. Theoretical Approaches to X-Ray Absorption Fine Structure. *Rev. Mod. Phys.* **2000**, *72*, 621.

(125) Zhuang, D.; Riera, M.; Schenter, G. K.; Fulton, J. L.; Paesani, F. Many-Body Effects Determine the Local Hydration Structure of Cs^+ in Solution. *J. Phys. Chem. Lett.* **2019**, *10*, 406–412.

(126) Riera, M.; Götz, A. W.; Paesani, F. The i-TTM Model for Ab Initio-Based Ion–Water Interaction Potentials. II. Alkali Metal Ion–Water Potential Energy Functions. *Phys. Chem. Chem. Phys.* **2016**, *18*, 30334–30343.

(127) Mancinelli, R.; Botti, A.; Bruni, F.; Ricci, M.; Soper, A. Hydration of Sodium, Potassium, and Chloride Ions in Solution and the Concept of Structure Maker/Breaker. *J. Phys. Chem. B* **2007**, *111*, 13570–13577.

(128) Berendsen, H.; Grigera, J.; Straatsma, T. The Missing Term in Effective Pair Potentials. *J. Phys. Chem.* **1987**, *91*, 6269–6271.

(129) DeMille, R. C.; Molinero, V. Coarse-Grained Ions without Charges: Reproducing the Solvation Structure of NaCl in Water Using Short-Ranged Potentials. *J. Chem. Phys.* **2009**, *131*, 034107.

(130) Klimeš, J.; Bowler, D. R.; Michaelides, A. Chemical Accuracy for the Van der Waals Density Functional. *J. Phys. Condens. Matter* **2009**, *22*, 022201.

(131) Sun, J.; Ruzsinszky, A.; Perdew, J. P. Strongly Constrained and Appropriately Normed Semilocal Density Functional. *Phys. Rev. Lett.* **2015**, *115*, 036402.

TOC Graphic